Foundation Technologies for Offshore Deep Water Renewable Energy

Abstract:

Floating platforms for bearing offshore wind turbines are fast becoming required to produce renewable energy from the wind capacity in the Atlantic, Mediterranean and deep North Sea. These platforms can be attached by way of mooring lines and anchors embedded in the seabed. The purpose of this study was to investigate the reaction of the soil on different types of pile anchors. A numerical study of anchor piles was performed by using the finite element software Abaqus. Several two-dimensional and three-dimensional models were simulated with different pile lengths and embedded in soils with different failure criteria. First an elastic behaviour for the pile and soil was simulated. After, the analysis focused on the reaction of undrained, clayey soil with the failure criterion of Tresca. As well as axial, lateral and combined loads were examined. The effect of the pile length to diameter ratio was analysed in an undrained soil with constant and with varying cohesion.

1 Introduction

The use of renewable energy is one of the most crucial issues of our times. This is a consequence of global climate change (pollution, global warming,…). The wind energy market will be one of the key markets in the renewable energies sector in the future [1]. Compared to the onshore wind, the offshore wind has a higher wind resource. Another benefit is that 70% of the earth consists of water, which means a lot of available space for offshore wind turbines (OWTs) [3]. Another trend expected for the future is that the average distance to shore and the water depth will increase [4].

2 Floating offshore wind turbines

Sixty-three percent of the European OWTs are installed in the North Sea, 22.5% are situated in the Atlantic Ocean and the rest in the Baltic Sea [5]. The Atlantic, Mediterranean and deep North Sea waters have a large wind capacity but the problem is that water depths in these areas are too great to install fixed offshore foundations. That is why other new concepts are being developed that utilizes floating support structures moored to the seabed [4]. The principle advantage of deep water sites is that higher wind resources and more stable winds are present in comparison with shallow water sites. Floating platforms do not require significant foundations (only the anchors of the mooring lines in the seabed) which means that nuisance from the installation of the foundations can be minimized and the structures are less dependent on the soil conditions. In addition, disturbance of sea life is reduced which is better in terms of potential environmental impacts [6].

A lot of useful offshore research has already been undertaken by the offshore oil industry. The results of this research can be used for the design of foundations from OWTs. In this industry, floating platforms have existed for 30 years. Most of these platforms can be used for OWTs too. These types of platforms are divided into three groups: spar buoys, tension leg platforms and semi-submersibles, Figure 1. This subdivision is based on the way the platforms achieve stability [4,7].

3 Anchoring systems

Floating wind turbines can be anchored to the seabed by a number of methods. The choice of the anchor system depends on the size and nature of the OWT, the environmental conditions, the mooring system, the geotechnical properties of the seabed and any financial or installation limitations. There are two different main types of anchors: gravity anchors and embedded anchors. Before designing and optimizing the mooring and anchoring system, there has to be an analysis of the site and soil data [8].

Gravity or box anchors are the oldest form of anchors. Anchoring is provided partly by the weight of the ballast and partly by the friction that develops between the seabed and the dead weight, Figure 2.

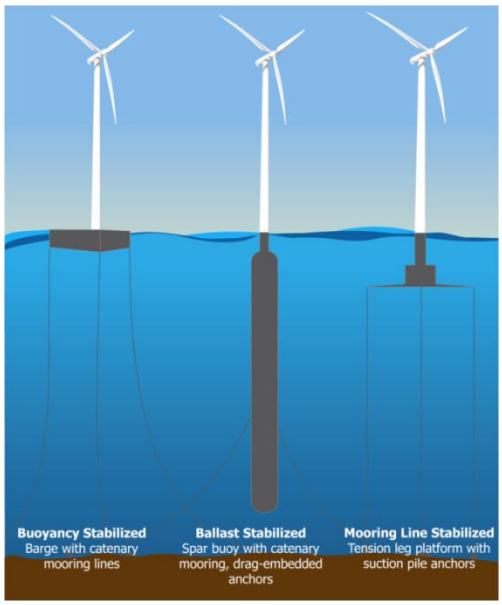

Figure 1 – The three main types of deep water wind turbine platforms: semi-submersible, spar buoy and tension leg platform [7]

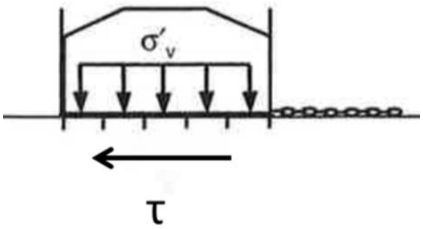

Figure 2 - Box anchor (gravity anchor) [9]

The different types of embedded anchors are: pile anchors, vertically loaded anchors (VLA), drag embedded and normal plate anchors, suction anchor and suction embedded plate anchors (SEPLA), Figure 3 and 4.

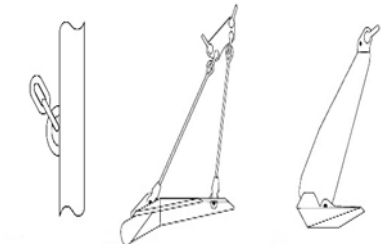

Figure 3 – From left to right: anchor piles – VLA – drag anchors [8]

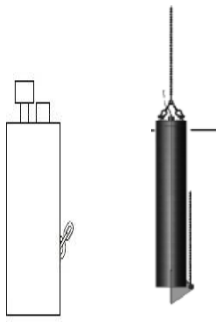

Figure 4 – Suction anchor (left) and SEPLA [8, 10]

The anchor pile is the subject of further analytical study here. The holding capacity is generated, just like a pile foundation, by the friction between the soil and the anchor. To have enough holding capacity, the pile has to be installed at a sufficient depth below the seabed. The pile can withstand both horizontal and vertical loads [8].

According to the way the pile anchors are installed, there are two different kinds of anchors: the driven pile anchor and grouted piles. The driven pile anchor is the most commonly used anchor in the offshore oil production. This anchor is driven into the seabed by a large hammer. Grouted pile anchors are, for example, used in rocks due to the fact that this ground is too hard for driven piles. The only way to secure an anchor in rock is to drill an oversized hole and then grout the inserted pile.

4 Mooring systems

There are two types of mooring systems: catenary mooring and taut leg mooring, Figure 5.

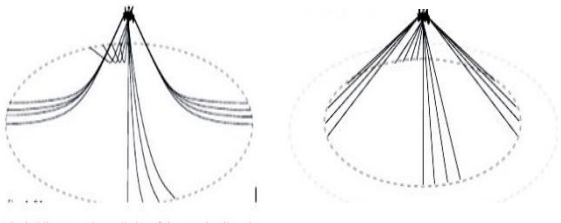

Figure 5 – Catenary system (left) and taut leg mooring [17]

Catenary mooring system is mostly used in water depths under 1000 m. A significant length of the lines lies on the seabed, leading to the

anchor being loaded in a horizontal direction. In contrast the taut leg mooring system is mostly used in water depths deeper than 1000 m. These mooring lines make an angle with the seabed. In that way, no lines are lying down on the seabed. That is the reason the anchors of the taut leg system are loaded in a vertical and horizontal direction.

Another consideration is the different ways to anchor the mooring lines to the anchors. In the first method, the chains are attached on the side of the pile. A second method involves grouting the chains into the upper part of the pile. The optimal attachment point for the anchor chain is below the mudline for both catenary and taut leg mooring system. The mooring system and the interaction with the soil will determine the angle of loading the anchor [9]. In this study the loads will be applied on the head of the pile anchor.

5 Soil classification

An undrained, cohesive soil is considered and the Tresca failure criterion was used.

While applying a load on a soil, the pressure within the soil will change. The change in the total stress will be equal to the sum of the change in the effective stress and the change the water pressure [11].

In clayey soils, there will be no immediate volume change, so the response is undrained. The load will be carried by the pore fluid, not by the soil particles. In the moment the soil is loaded, the changes in the water pressure will be equal to the changes in the total pressure. The effective stress will not change [11].

The behaviour of clay can be described in three steps [11]:

- Step 1: Initial undrained compression;
- Step 2: Primary consolidation: the change in total stress caused by the loading transfers from the pore water to the soil skeleton (effective stress changes); with an associated change in volume with time;
- Step 3: Secondary consolation occurs after complete dissipation of the pore water pressure, some settlement of the soil will continue to take place due to the plastic behaviour.

The focus in this study is the undrained failure of the soil-structure for lateral, axial and combined loadings. Using the program Abaqus [12], the response of the piles will be analysed. The geotechnical modelling has been developed progressively, starting with an elastic pile with elastic soil around it. Subsequently, an elastic pile in a soil modelled as an elastic-plastic material was considered. Three elasto-plastic models were initially considered – Tresca, Mohr-Coulomb, and Drucker-Prager however severe difficulties were experienced in implementing the latter two and thus, the studies here only consider the Tresca model. The Tresca model can be used to simulate the undrained response of cohesive soil.

The Tresca failure criterion can be considered as a particular case of the Mohr-Coulomb failure criterion. In Abaqus, the Tresca model has to be implemented as a Mohr-Coulomb model because Abaqus defines the Tresca model as a pressure-independent Mohr-Coulomb model with $\varphi = 0°$ [12]. The Mohr-Coulomb criterion is widely used to simulate the inelastic behaviour of soils under drained conditions, i.e. in terms of effective stress. The limiting soil shear strength, τ defined by the model is described by:

$$\tau = c' + \sigma'.\tan\varphi' \qquad \text{Eq. 1}$$

In an undrained analysis, the angle of shearing resistance of the soil, φ', is by definition zero and the Mohr-Coulomb criteria reduces to the special case of the Tresca model. In this model, the soil strength is described by the undrained shear strength, s_u or c_u, equation 2.

$$\tau = s_u\ (= c_u) \qquad \text{Eq. 2}$$

Another property of the undrained analysis is that the shear strength is independent of confining stress and the analysis is undertaken in terms of total stress. In an undrained analysis, the pore water pressures are not known. Figure 6 represents the assumption made in terms of shear strength for an undrained analysis [13].

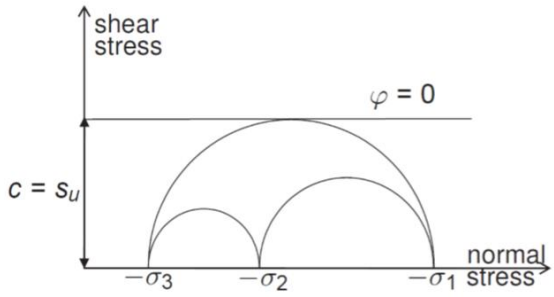

Figure 6 – Tresca criterion using undrained (total stress) strength parameters [13]

6 Numerical model: Elastic model

The numerical simulation of the pile anchors was carried out using the finite element program Abaqus. Both two-dimensional (2D) and three-dimensional (3D) piles with different dimensions were simulated. The dimensions of the pile are expressed in terms of the length to diameter ratio, L/D. The L/D-ratios considered here are 10, 20 and 40. Since the diameter of the pile is constant and equal to 1 m, the length of the piles was defined by the L/D-ratio. To make the simulation easier, the piles were represented by solid elements with stiffness properties of the solid elements adjusted in order to provide a similar bending stiffness to a hollow steel pile. The Poisson's ratio, ν, of the steel is taken 0.2. The wall thickness of the pile is considered to be 20 mm. The interaction between the pile and the soil is defined as a rough contact.

The main target of the elastic models was finding progressively a good model and mesh to simulate the pile embedded in the soil. The settlements calculated by both 2D and 3D models were compared with theoretical values from [15].

It was found that a distance from the pile toe to the bottom of the soil of 30 times the diameter and a distance from the pile axis to the side of the soil of 50 times the diameter gave good results without a significant distortion of the calculation. The parameters of the elastic soil are a Young's modulus, E of 40 MPa and a Poisson ratio, ν of 0,5.

After comparing the obtained values from the FEA with the theoretical values, there could be concluded that different types of elements gives different results. The 2D model is defined by quadratic elements with a second-order interpolation and the 3D model by linear elements with a first-order interpolation. The difference is that in a first-order interpolation a constant volumetric strain is considered throughout the element. In contrast to the second-order elements which will have a higher accuracy when the problem doesn't involve a lot of distortion [12]. The difference between the settlement of the 2D model and the theoretical value is for the 10 m long pile an a load of 400kN, 2.5% relative to the theoretical value, for the 3D model is this percentage -2.9%. The difference between the 2D and 3D value is 5.3% relative to the 3D model. For the other lengths are the percentages similar.

Further, there is also found that smaller elements can improve the results, however they lengthen the run time extensively. A good equilibrium between the run time and the quality of the results is a requirement. Taking these conclusions into account, the simulated models can be used further to analyse the reaction of the soil.

7 Numerical model: Tresca model

Subsequently, an elastic pile in a soil modelled as an elastic- perfectly plastic material was considered, more specifically, the Tresca model was used to simulate the undrained response of clayey soil.
The elastic parameters of the steel and the soil are the same as in the elastic models. Next to these parameters, the cohesion, equal to the undrained shear strength, had to be defined. Two different soil conditions were considered; soil with a constant undrained shear strength of 60 kPa (Soil Model 1) and soil with the undrained shear strength increasing with depth (Soil Model 2). In Soil Model 2, the profile of undrained shear strength had a value of 5 kPa at the surface and it increased at a rate of 1.5 kPa per meter.

7.1 Axially loaded pile

Firstly, the load-displacement graphs Figure 7 were examined for piles under axially loading.

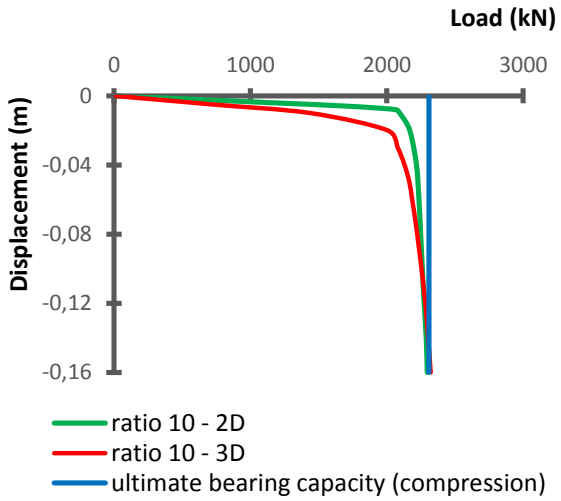

Figure 7 – Soil Model 1: Load-displacement graph of a pile with L/D-ratio 10

The load-displacement response shown in Figure 7 presents the displacement of the top of the pile when the load at the pile head increases and compares the results of 2D and 3D FEA, and the ultimate resistance estimated based on an analytical expression for pile capacity. Similar behaviour was seen in all lengths analysed and in Soil Model 2. Also the tension load gave the same curves with a positive displacement.

The bearing capacity of the axially loaded pile has to be distinguished in the capacity for compression and for tension. The pile capacity for compression loading can be defined as the sum of the ultimate pile base resistance and the shaft resistance. Accordingly, for a tension load, the bearing capacity is the sum of the shaft resistance and the weight of the pile.

7.2 Laterally loaded pile

After, the laterally loaded piles were examined. The Broms method was considered to calculate the ultimate lateral load on the head of the pile. This method makes a difference between short, rigid and long, flexible piles. Short, rigid piles will act as one unit when a lateral load is applied and failure will be governed by the soil strength. In contrast, long, flexible piles will fail structurally through the formation of a plastic hinge with perhaps some local soil yield only.

7.2.1 Relative stiffness

A way to define the relative stiffness of the pile-soil system is the elastic Vesic theory. Therefore the reaction modulus of the soil k, has to be calculated.

$$k = 0.65 \sqrt[12]{\frac{E\,B^4}{(EI)_f}} * \frac{E}{(1-\nu^2)} \qquad \text{Eq. 3}$$

The distinction between flexible, semi-flexible and rigid for free-headed piles in a uniform soil (Soil Model 1) is determined by the parameter λL, equation 4.

$$\boldsymbol{\lambda} = \sqrt[4]{\frac{\mathbf{k}}{\mathbf{4(EI)_f}}} \qquad \text{Eq. 4}$$

A pile with λL larger than 3 is defined as a flexible pile, between 1 and 3 as a semi-flexible pile and smaller than 1 as a rigid pile. Using this method, it can be concluded that for Soil Model 1 the pile with L/D-ratio 10 has to be considered as a semi-flexible pile. In contrast to the others which will behave as long piles.

For a free-headed pile in a soil with a modulus of reaction increasing with the depth (Soil Model 2), the distinction is determined by the parameter ηL, with η defined by equation 5.

$$\eta = \sqrt[5]{\frac{\mathbf{n_h}}{\mathbf{(EI)_f}}} \qquad \text{Eq. 5}$$

A pile with ηL larger than 4 is defined as a flexible, long pile, between 1.5 and 4 as a semi-flexible pile and smaller than 1.5 as a short, rigid pile. Using this method for the soils with the varying undrained shear strength, the pile with a length of 10 m is defined as a semi-flexible pile and the piles with a length of 20 m and 40 m will behave as long piles. All these statements about the relative stiffness from the pile-soil systems can be confirmed by the deflection graphs of the laterally loaded piles.

7.2.2 Broms and modified method

Broms states that for a pile in cohesive soil, static equilibrium can be demonstrated by accepting a uniform soil resistance, p along the length of the pile of $9c_ub$ (c_u is the undrained shear strength and b is the diameter of the pile).

Near the surface, the soil resistance is ignored over a distance of 1.5b as shown in Figure 8 (the blue area). That is because in that zone, the soil can move up and out when the pile is bending due to the lateral load. Therefore it would give no resistance anymore. The ultimate laterally load can be calculated from the horizontal and the moment equilibrium [14].

Another method to calculate the ultimate laterally load is the modified method from [16]. The difference with the Broms method is the distribution of soil resistance. Also in this method is the ultimate laterally load obtained by the horizontal and moment equilibrium of the soil resistance. Figure 8 shows the distribution in both the Broms (blue area) and the modified method (black area).

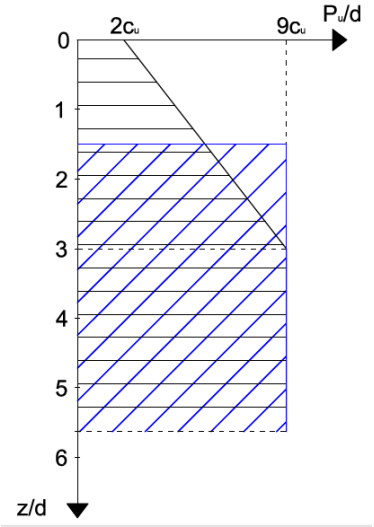

Figure 8 – The distribution of the soil resistance of the Broms method and the modified method

In Table 1 the results from the FEA are presented and compared to the theoretical results from both the Broms and the modified method.

Table 1 – Soil Model 1: lateral bearing capacity for piles

L/D-ratio	Ultimate load, kN		
	Broms method	Modified method	FEA 3D
10	1512	1692	2900
20	1705	1892	4500
40	1705	1892	5100

The ultimate lateral load resistance obtained from the simulations is larger than the theoretical values. For the long piles that can be explained by the fact that they are theoretically limited by the moment resistance of the pile section where in the analyses pile yield is not considered due to the elastic behaviour. The maximum bending moment from the pile with L/D-ratio 10 is not limited by the yield moment and the lateral load of the final stage of the elastic pile analysis is still larger than the ultimate lateral load defined by the theoretical methods. This difference may be attributed to the contact definition between the pile and the soil which is completely rough, so the pile and the soil are not able to separate in contrast to what is assumed in the theoretical models, Figure 9. This will also enlarge the ultimate lateral load of longer piles.

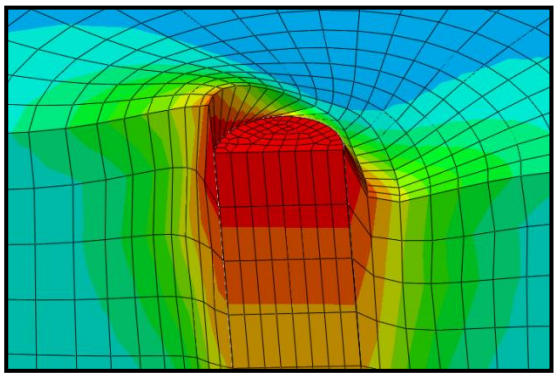

Figure 9 – Soil Model 1: The simulated contact between the pile and the soil from the pile with L/D-ratio 20

7.2.3 Deflection

In Figure 10 is the deflection graph of the FEA models with L/D-ratio 20 shown. The green curve (Soil Model 1) and the brown curve (Soil Model 2) represent the deflection profile from the FEA at the stage when the maximum bending moment is mobilized approximately equal to the yield moment.

The deflection profiles of the FEA for the load that mobilizes the yield moment are compared with the deflection profiles calculated by the Winkler method. This method considers two different cases: the first is a uniform soil with a constant reaction modulus k (Soil Model 1) and the second is a layered soil with a reaction modulus which is varying linear with the depth (Soil Model 2) [17].

The blue curve in Figure 10 shows the deflection profile for Soil Model 1 calculated by the Winkler equations [17]. For Soil Model 2 only the deflection on the pile head is calculated by the Winkler method: 0.22 m. This value will be compared with the value of the FEA (0.28 m). The conclusion is that in both cases the deflection calculated by the Winkler equations is smaller than the deflection of the FEA. The reason of this discrepancy will be explained in Section 7.2.5. The red and the purple deflection curves show the displacement at the final stage of the elastic pile analysis for Soil Models 1 and 2 respectively.

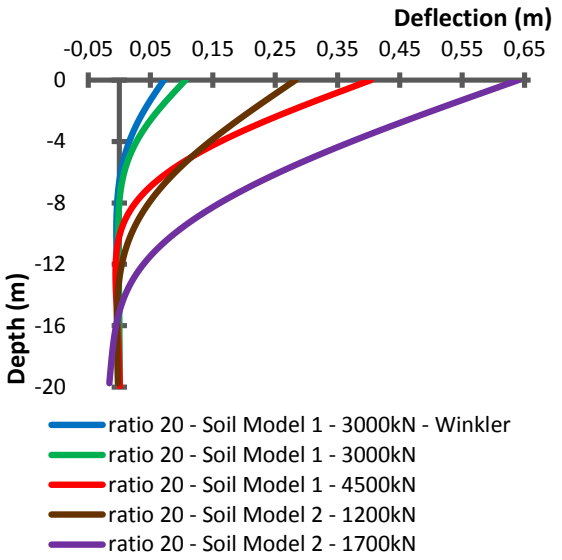

Figure 10 – Deflection curves of the laterally loaded pile with L/D-ratio 20

7.2.4 Bending moments

The bending moments at the final stage of the elastic pile analysis (red curve in Figure 11) are larger than the theoretically calculated bending moments which are equal to the yield moment of 5251 kNm (blue curve in Figure 11) for the long, flexible piles. That can be explained by the fact that the FEA is not limited by the moment resistance of the pile section and by the contact definition, Figure 9. According to the short, rigid piles the bending moment of the last stage of the elastic pile analysis will be larger than the yield moment for piles in Soil Model 1 and smaller than the yield moment for piles in Soil Model 2.

The stage from the FEA that mobilizes a bending moment close to the yield moment (5250 kNm) is presented by the blue curve in Figure 11. The lateral load that is mobilizing the yield moment is equal to 3000kN for the pile with L/D-ratio 20 and the Soil Model 1. This load can be compared with the lateral load of the Broms method: 1705kN (Table 1). The loads of the FEA are still larger than the loads of the Broms method which can be explained by the fact that there will be more soil resistance because no gap formation has been modelled.

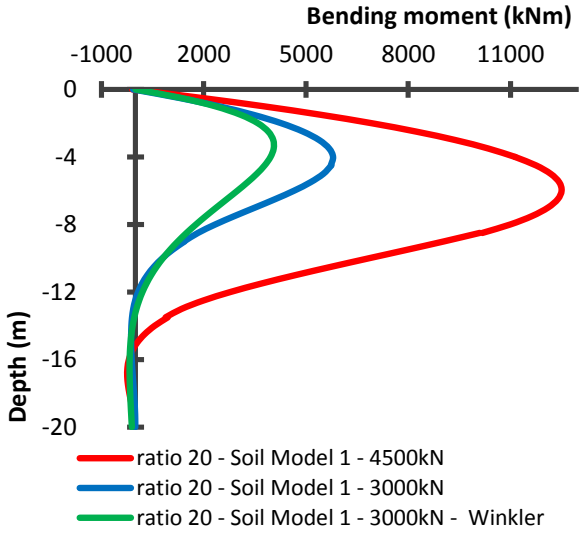

Figure 11 – Soil Model 1: Bending moment of the laterally loaded piles with L/D-ratio 20

The loads of Soil Model 2 cannot be compared with the loads of the Broms method because the Broms method is only valid for uniform soils. Further, there can be concluded that the yield moment of the piles with Soil Model 1 will be reached faster.

Just like the deflection curve, also the bending moments will be compared with the Winkler method [17]. The bending moments, taking into account the lateral load where the theoretical maximum moment is about equal to the yield moment, is for Soil Model 1 presented by the green curve in Figure 11. For Soil Model 2 only the maximum bending moment and its depth are calculated and compared with the FEA. In both cases is the maximum bending moment of the FEA and its depth larger than those of the Winkler method. The reason for this purpose is given in Chapter 7.2.5.

7.2.5 Soil resistance along the pile

A way to check the limiting pressure along the pile is the method of [16]. The limiting bearing factor is defined as the division of the

limiting pressure by the undrained shear strength and the diameter of the pile. [16] states that the limiting bearing factor of a perfectly rough pile 11.94 is. Figure 12 shows the contact pressure of the section of the laterally loaded pile with L/D-ratio 20, 1 m below the soil surface.

In Figure 13 the limiting factors evaluated at 1 meter intervals along the pile with L/D-ratio 20 and Soil Model 1 are presented by the blue curve. Also shown are the distribution of the lateral pressures assumed by Broms and the modified method; these have much lower values than those obtained from the FEA. This discrepancy can be explained by the fact that the Broms and modified method only assume the compression because there should be a gap where the tension is occurring in Figure 12. The lower part with negative limiting bearing factors (below 10 m depth, Figure 13) is ignored in the Broms and modified method for long piles.

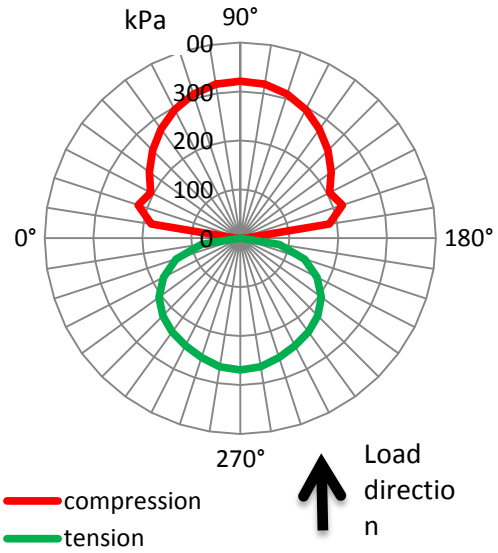

Figure 12 – Soil Model 1: Soil resistance at 1 m depth for pile with L/D-ratio 20

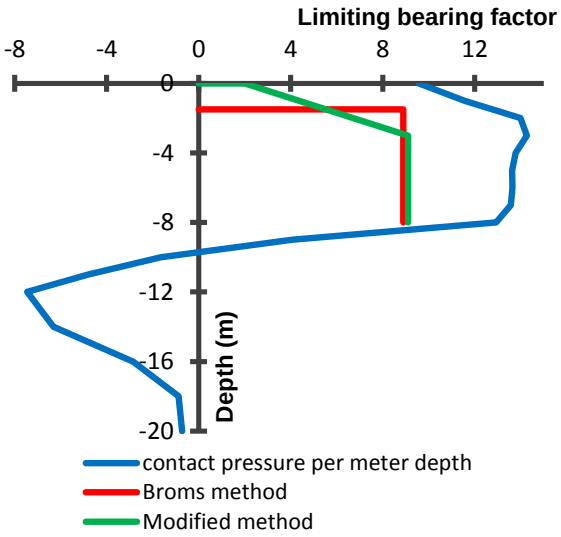

Figure 13 – Soil Model 1: Soil resistance along the pile from the pile with L/D-ratio 20

The reaction modulus k can be calculated by the division of the contact pressure, p determined above, by the deflection at the same depth. The reaction modulus will not be constant as was assumed for the calculations of the bending moment profiles, Figure 11 and the deflection profiles, Figure 10. The initial reaction modulus calculated by equation 3 was larger compared with the reaction moduli referred from the FEA in the upper part of the pile.

The equations used to calculate the constant reaction modulus are based on Vesic elastic theory. In this case, there will be plasticity developing which gave a lower effective reaction modulus.

If we compare the deflections and bending moments calculated with different reaction moduli, there can be concluded that the smaller the reaction modulus, the larger the deflections and the bending moment, and the depth to the maximum moment will increase. That explains also the smaller deflection and bending moment calculated with the Winkler method in Figure 10 and Figure 11. There was also found that the reaction modulus that fits the best with the deflection profile of the FEA will be another reaction modulus than the one that fits the best with the bending moment profile of the FEA. That confirms that the reaction modulus cannot be considered constant.

7.3 Combined loading

Pile anchors with taut leg mooring system are used for the transfer of both axial and lateral loads into the ground. So it will be of interest to examine the combined loading of piles in the soil.

In Figure 14, the interaction between combined loads is shown for Soil Model 1. There can be seen that the horizontal load will not affect the vertical tension capacity a lot, except when the tension is very close to the ultimate value. That can be explained by the difference in mechanism. Axial loading involves the whole pile shaft interface acting in shear, while the lateral loading involves compression and shearing of a soil mass perpendicular to the interface over a limited depth.

The dotted lines in Figure 14 represent the interaction diagrams based on failure loads extrapolated from the FEA with the method described in [18].

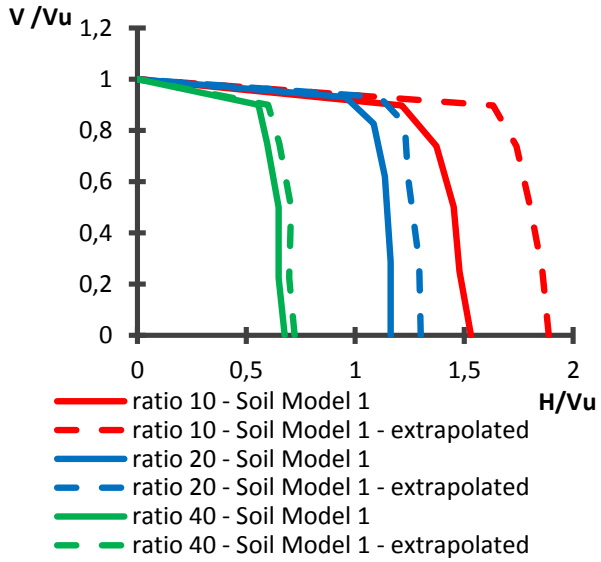

Figure 14 – Soil Model 1: Ultimate load interaction diagram for piles

Figure 15 show the ultimate load interaction curve and the extrapolated curve for the L/D-ratio 10 and Soil Model 1. Besides this, the green curve presents the interaction curve where the combined load mobilizes the yield moment of the pile. There can be concluded that the structural yield occurs before the geotechnical failure, however this is a semi-flexible pile. Only for a large tension load is the geotechnical failure reached before the yielding of the pile. For the 10 m long pile embedded in soil with varying cohesion (Soil Model 2), the geotechnical failure will occur before the yielding of the pile in all cases since the bending moment at the last stage of the elastic pile analysis is smaller than the yield moment.

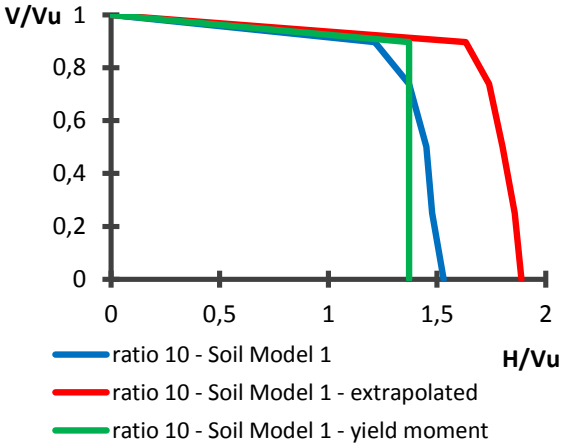

Figure 15 – Ultimate load interaction diagram for the piles with L/D-ratio 10 and soil with constant undrained shear strength

8 Conclusions

It can be concluded that depending on the relative stiffness of the pile-soil system, the model will fail by geotechnical failure or by yielding of the pile. In a case of doubt, both have to be examined.

Another conclusion is that some care has to be taken in using certain methods to simulate the pile-soil interaction at the Ultimate Limit State (ULS). It was shown for the Winkler method that there may be an incompatibility in terms of predicted displacement and bending moment when assuming a constant reaction modulus.

When combined tension and lateral loads are applied to a pile there is little interaction between one and the other in terms of ultimate resistance. Thus for short, rigid piles, the full ultimate horizontal soil resistance can be relied on when deriving the design horizontal resistance. For long, flexible piles, the lateral resistance is governed by the strength of the pile section.

9 References

[1] REN21. (2014). *Renewables 2014 – Global status report* (1st ed.). Retrieved from REN21 website: http://www.ren21.net/portals/0/
[2] documents/resources/gsr/2014/gsr2014_full%20report_low%20res.pdf
[3] Implementation of a 2MW Deep Offshore Wind Demonstration Project. (2013, July). Paper presented at The WindFloat Project- Public Session of edp, Apúlia.
[4] European Wind Energy Association. (2015, January). The European offshore wind industry – key trends and statistics 2014 (1st ed.). Retrieved from EWEA website: http://www.ewea.org/fileadmin/files/library/publications/statistics/EWEA-European-Offshore-Statistics-2014.pdf
[5] Schaumann, P., Lochte-Holtgreven, S., & Steppeler, S. (2011). Special fatigue aspects in support structures of offshore wind turbines. Besondere Aspekte hinsichtlich der Materialermüdung bei Tragstrukturen von Offshore-Windenergieanlagen. Materialwissenschaft und Werkstofftechnik, 42(12), 1075-1081. doi: 10.1002/mawe.201100913
[6] Williams, A. (2011, May 3). A Buoyant Future for Floating Wind Turbines? Retrieved from http://www.renewableenergyworld.com/rea/news/article/2011/05/a-buoyant-future-for-floating-wind-turbines
[7] Cichon, M. (2011, June 21). DeepCwind tirelessly developing floting offshore wind. Retrieved from http://www.renewableenergyworld.com/rea/news/article/2011/06/deepcwind-project-tirelessly-developing-floating-offshore-wind
[8] Vryhof anchors. (2010). Anchor Manual 2010 – The Guide to Anchoring. (4rd ed.). Yssel, The Netherlands. Retrieved from http://www.vryhof.com/anchor_manual.pdf
[9] Di Emidio, G. (2014). Offshore foundations. Ugent, laboratory of geotechnics.
[10] Gaudin, C., O'loughlin, C., Randolph, M., & Lowmass, A. (2006). Influence of the installation process on the performance of suction embedded plate anchors. Géotechnique, 56(6), 381-391.
[11] Randolph, M., & Gourvenec, S. (2011). Offshore geotechnical engineering: CRC Press.
[12] Manual Abaqus 6.14
[13] STROMBLAD, N. Modeling of Soil and Structure Interaction Subsea.
[14] Reese, L. C., & Van Impe, W. F. (2000). Single piles and pile groups under lateral loading: CRC Press
[15] Poulos, H. G., & Davis, E. H. (1980). Pile foundation analysis and design.
[16] Fleming, K., Weltman, A., Randolph, M., & Elson, K. (2008). Piling engineering: CRC press.
[17] Bowles, J. E. (1988). Foundation analysis and design.
[18] Chin, F. (1972). The inverse slope as a prediction of ultimate bearing capacity of piles. Paper presented at the Proceedings of the 3rd southeast Asian conference on soil engineering, Hong Kong.